Modelling the hydrodynamic support of cylinder bore and piston rings with laser textured surfaces

Eduardo Tomanik*

MAHLE Brazil Francisco J. Profito, Demetrio C. Zachariadis-Polytechnic School-University of São Paulo, Brazil

A B S T R A C T

An one-dimensional computer model was used to simulated surface texture effects on engine cylinder bore, top and oil control rings. Steady state, reciprocating tests and engine conditions were considered. For the engine simulation, conditions close to the top reversal and at mid-stroke were simulated. Different micro-dimple geometries were considered, as well as full and partial texturing. As main conclusion, micro-dimples on the bore and rings were able to generate significant hydrodynamic support with potential to reduce both friction and wear. A special benefit was predicted when the micro-dimples were on the flat surface of the oil control rings.

© 2012 Elsevier Ltd. All rights reserved.

1. Introduction

Growing attention has been directed to friction reduction in internal combustion engines in order to attend an ever-increasing stringent CO_2 emissions legislation. Friction losses in such equipments account for approximately 10% of the total fuel consumption [1]. Although the specific friction share among the components depends on engine design, operating conditions and other factors, it is generally accepted that the main friction contributor is the piston-cylinder system. Cylinder bore finish and piston Oil Control Ring (OCR) properties are the most promising friction reduction features to be coped with.

Several experimental and theoretical researches have investigated the benefits of using micro-textures as a surface finishing technique for tribological improvements, i.e. friction and wear reduction, on several engineering applications [2–15]. Such improvements are related to the following effects:

- *Micro-bearing*: textures work as micro-bearings generating hydrodynamic pressures even among parallel flat surfaces.
- *Oil reservoir*: textures work as lubricant micro-reservoirs attenuating critical lubrication conditions.
- *Debris trap*: textures work as micro-traps storing and avoiding the presence of abrasive and debris at the contact interface, hence reducing wear. See Fig. 1.
- *Scratches stopper*: An eventual hard particle or an asperity in contact will, at least momentarily, reduce contact when passing through the micro-dimple.

Laser Surface Texturing (LST) has become the most common technique employed to create micro-textures in typical engineering topographies. The geometry pattern usually adopted for the texturing consists in a succession of equally spaced circular dimples that can be either "fully" or "partially" distributed throughout the contact surfaces [2–4,6–8,10,15]. On both situations, the use of dimples is worth especially when the sliding surfaces are plane, making LST appealing for the flat faces of 2-piece oil control rings used in diesel engines but the oil ring running faces, 0.15–0.30 mm width, are too narrow for conventional texturing (50–100 μm dimple diameter). To the best of author knowledge, there is no published study of use of LST on OCRs.

More recently, 'femtosecond' laser technique [16] has been employed to obtain 1–5 μm diameter dimples which are small enough to be lined up on one or two rows on the contact face of oil control rings. The present work is intended to investigate the effects of LST on the cylinder bore, piston top rings and particularly on the Oil Control Ring running faces using a fairly simple mixed lubrication model. Simulation results concerning the hydrodynamic pressures generated due to the micro-bearing effects and their influence on contact and friction forces are considered in order to give insights into the application of LST on OCR.

2. Overview of the computational model

The hydrodynamic pressures are calculated solving the one-dimensional Reynolds equation derived from the Navier-Stokes equation by assuming the classical hypotheses of lubrication theory, i.e. the surfaces are admitted smooth and the magnitude

* Tel./fax: +55 11 5545 0892
E-mail address: eduardo.tomanik@br.mahle.com
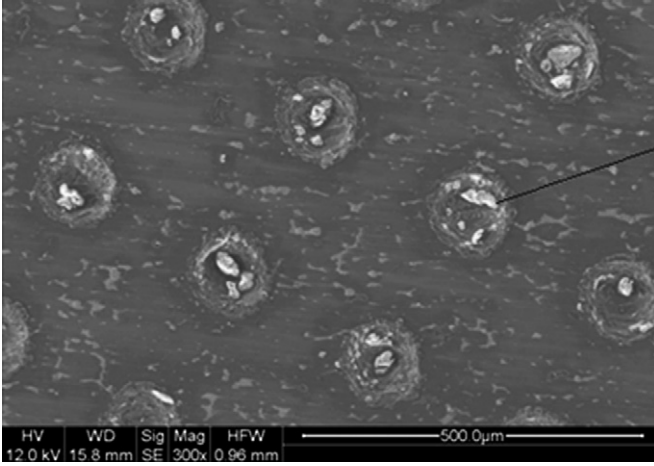
Fig. 1. Abrasive particles trapped within the micro-dimples after a bench test.

Fig. 2. Overview of the tribosystem idealized for the mathematical model proposed in present work [17–18].

of the thickness of the fluid film is small compared with the other ones at the contact interface. For an isothermal and incompressible lubricant, the one-dimensional transient Reynolds equation can be written as [17–19]:

$$\frac{\partial}{\partial x}\left[\frac{(H_2-H_1)^3}{12\mu}\frac{\partial p_H}{\partial x}\right] = \left[\frac{U}{2}\frac{\partial(H_2-H_1)}{\partial x}\right] + \left[-U\frac{\partial H_2}{\partial x}\right] + \left[\frac{\partial h_{min}}{\partial t}\right] \quad (1)$$

where p_H is the hydrodynamic pressure, μ is the lubricant dynamic viscosity, U is the sliding velocity of the mobile surface, H_1, H_2 describe the geometry of the delimiting surfaces and h_{min} is the minimum oil film thickness (see Fig. 2). The adoption of such one-dimensional model is in accordance with previously published works [20,21] in which it was presented as a consolidated one for piston ring simulations. In the present work, flow-factors are not employed as a means to estimate surface roughness effects, since the exact geometric description of the dimples is considered in the calculation of hydrodynamic pressure fields; thus, roughness properties only affect the evaluation of the contact forces. Accordingly, the resulting methodology, despite its limitations, incorporates the hydrodynamic effects caused by the dimples in the conventionally one-dimensional accepted piston ring model.

Temperature, pressure and shear rate influence on viscosity are modeled by the Vogel, Barus and Cross correlations, respectively. Combining such rheology models, viscosity is calculated as [17,18,22]:

$$\begin{cases} \mu(T,p_H,\dot{\gamma}) = a\exp\left\{\underbrace{\alpha_B p_H}_{pressure\ effect} + \underbrace{\frac{b}{T+c}}_{temperature\ effect}\right\}\underbrace{\left(\frac{1+(\mu_\infty/\mu_{pH})(\dot{\gamma}/(c_1+c_2 T))^m}{1+(\dot{\gamma}/c_1+c_2 T)^m}\right)}_{shear-thinning\ effect} \\ \alpha_B = \left[0.6+0.965\log_{10}(1000\mu_T)\right]10^{-8} \end{cases}$$
$$(2)$$

where T is the lubricant temperature (°C), $\dot{\gamma}$ is the lubricant shear rate, a, b, c are the empirical constants of the Vogel equation and c_1, c_2, m and $(\mu_\infty)/(\mu_{pH})$ are the empirical constants of the Cross equation. The viscosity corrections are performed implicitly in an iterative algorithm during the numerical solution. In this sense, the viscosity in Eq. (1) corresponds to an effective viscosity that describes the non-Newtonian properties of the lubricant. Such methodology is usually employed to solve mixed-elastohydrodynamic problems [23–25]. Additionally, the elastohydrodynamic effects are disregarded in the present analysis, justifying the incompressible lubricant assumption.
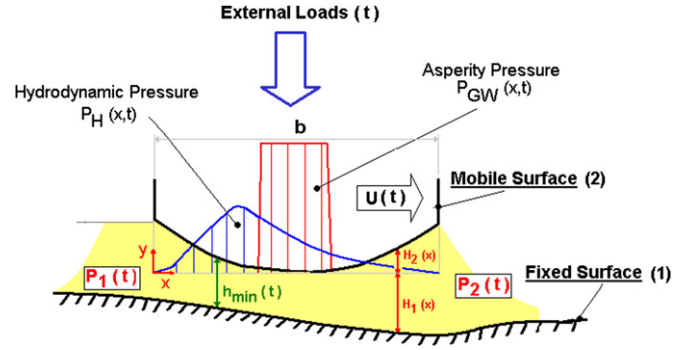
Cavitation effects are taken into account in the Reynolds equation by means of the complementary Swift-Steiber (or Reynolds) boundary conditions:

- The pressure gradient at the cavitation boundaries is zero:

$$\frac{\partial p}{\partial n} = 0; \quad \text{(cavitation boundaries)} \quad (3)$$

- The pressure within the cavitation regions is constant and equal to the vapor/gas-pressure of the lubricant (p_{cav}):

$$p \to p_{cav} = 0; \quad \text{(within the cavitation regions)} \quad (4)$$

As the cavitation boundaries are unknown a priori, the solution is carried out employing iterative methods, like the one based on the Finite Difference Scheme (FDS) with Successive Over-Relaxation (SOR) procedure [17,18]. In this case, the cavitation boundaries are automatically found setting to zero all pressures below p_{cav} [26]. Although this cavitation model does not satisfy mass-conservation of the lubricant flow throughout the cavitation boundaries [27], it has been employed in several publications as a valid means for the calculation of the hydrodynamic load carrying capacity generated in textured surfaces [3,5,7,13,14].

Wherever the lubricant film is thin enough, asperity contact takes place and contact pressures are calculated by the Greenwood and Tripp equation [28–31]:

$$p_{ASP}(x,t) = \begin{cases} \frac{16\pi\sqrt{2}}{15}E^*(\eta^2\beta^{3/2}\sigma^{5/2})F_{5/2}\left[\overline{h}(x,t)\right], & p_{ASP} \le 3\sigma_{esc} \\ 3\sigma_{esc}, & p_{ASP} > 3\sigma_{esc} \end{cases} \quad (5)$$

where p_{ASP} is the asperity pressure, $\overline{h} = h - Z_s/\sigma$ the dimensionless clearance between the mating surfaces, $Z_s = \sqrt{Z_{s_1}^2 + Z_{s_2}^2}$ the combined asperity summits mean height, $\sigma = \sqrt{\sigma_1^2 + \sigma_2^2}$ the combined asperity summits height standard deviation, $\beta = \sqrt{(1/\beta_1^2)+(1/\beta_2^2)}$ the combined asperity summits mean radius, $\eta = \sqrt{\eta_1^2 + \eta_2^2}$ the combined asperity summits density, $E^* = E_1 E_2/(E_1(1-v_2^2)+E_2(1-v_1^2))$ the composite elastic modulus, v the Poisson's ratio and σ_{esc} the tensile strength of the softer surface. The subscripts denote each rough contact surface.

The total friction force is a combination of the viscous and the asperity contact effects:

$$f_{total}^{fric}(t) = L\left\{\underbrace{\int_0^b\left[\frac{(H_2-H_1)}{2}\frac{\partial p_H}{\partial x} + \frac{\mu U}{(H_2-H_1)}\right]dx}_{hydrodynamic\ friction} + \underbrace{\overline{\mu}_b\int_0^b[p_{ASP}(x,t)]dx}_{asperity\ contact\ friction}\right\}$$
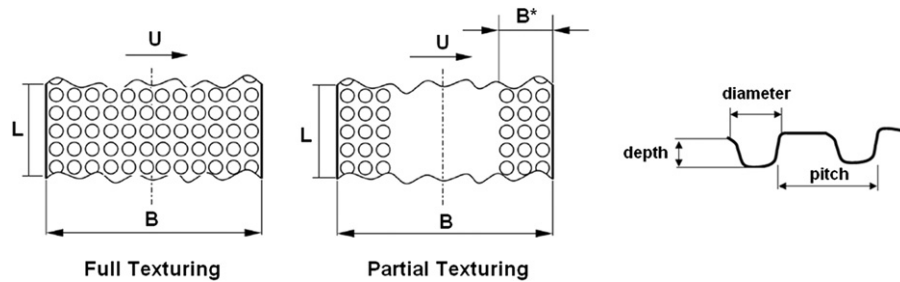$$(6)$$

Fig. 3. Distribution and dimensions of dimple texturing.

where $\overline{\mu}_b$ is the boundary friction coefficient, which must be known a priori; in this work $\overline{\mu}_b = 0.12$ was adopted based on previous experiments with piston rings [32].

A computer code named MAHLE-VTL[1] (Virtual Tribology Laboratory), written in MATLAB® was developed using the described equations. At each time-step, the equilibrium between the applied load and the sum of hydrodynamic and asperity loads is calculated iteratively using the Newton–Raphson method. The code was developed mainly to predict and comprehend results of reciprocating tribological bench tests such as the effects of changes on load, speed, roughness, oil viscosity and temperature. More details about the code and validations for non-textured surfaces are described in [17,18].

3. Simulations with textured profiles for cylinder bore, top and oil control rings

In order to investigate the use of surface texturing on piston rings, some numerical simulations were carried out employing the described model. When textured, the running face of the piston rings was assumed flat and with micro-dimples fully and partially distributed-see dimples distribution and dimensions in Fig. 3. CPU time was reduced by assuming "fully flooded" lubrication conditions. Successive more realistic cases will be described, starting from steady state conditions, then simple reciprocating bench tests and finally combustion engine conditions. Table 1 describes the ring and bore surface parameters, based on measurement of actual parts [29,31,32]. The ring, being much smoother than the bore, was assumed smooth.

3.1. Steady state simulations

As a first approach, some steady-state simulations were performed. A 0.6 m/s mobile surface (textured) velocity was adopted, the external load force was fixed to 50 N, resulting in an equivalent pressure around 1.70 MPa and the lubricant is SAE30 at 30 °C. Table 2 summarizes the values of the minimum oil film thickness, hydrodynamic load carrying capacity and the percentage of hydrodynamic support calculated for each texturing variant. Higher load carrying capacity was always observed for partial texturing, especially for the variant with smallest dimples pitch, i.e. the 100_10_150 variant. Fig. 4 illustrates the hydrodynamic and asperity contact pressures for the 100_10_150 texturing variant.

The individual effects of the micro-dimples are important for full texturing configurations (see Fig. 4a). The maximum hydrodynamic pressures are observed at the convergent regions of the dimples, where the "wedge" effect takes place (micro-bearing effect). Further, it is interesting to point out the generation of

Table 1
Surface parameters.

	E (GPa)	σ_{esc}(MPa)	$v(-)$	Z_s (μm)	σ (μm)	β (μμm)	η (m^{-2})
Ring	250	500	0.30	0	0	0	0
Bore	120	250	0.30	0.33	0.25	13.1	3.5 E10

Table 2
Simulation results. Steady-state condition, velocity 0.6 m/s and load force 50 N.

Texturing distribution diameter_depth_pitch (μm)		Texturing variant		
		100_10_150	100_10_250	100_10_450
Minimum oil film thickness (μm)	Full	0.90	0.94	0.93
	Partial	1.80	1.33	1.04
Hydrodynamic load carrying capacity (N)	Full	34.9	36.6	33.6
	Partial	50.0	50.0	47.7
Hydrodynamic support (%)	Full	69.9	73.2	67.1
	Partial	100	100.0	95.3

hydrodynamic pressures even in the flat portions between each micro-dimple. Such effect occurs due to the non-zero pressures observed upstream each dimple, making these intermediate flat regions work like micro-hydrostatic bearings with linear pressure distribution.

For partial texturing, the collective effects of the micro-dimples are observed by the "accumulation" of hydrodynamic pressure at the initial textured portion on the right side of the flat profile (see Fig. 4b). This "accumulation" of pressure is generated due to a mechanism similar to the inlet roughness concept [33] in which the partial texturing creates an "effective clearance" reduction in the sliding direction. In other words, the mean difference of geometry between the textured and non-textured portions creates an "equivalent Rayleigh-step" (see Fig. 5) that generates significant hydrodynamic pressures. Such collective effects result in higher load carrying capacity than the individual effect described for full texturing [5]. In this sense, partial texturing should be recommended for flat piston rings regardless of the position of the textured portions [3,4,6–8,10].

3.2. Comparison between barrel shaped and flat textured piston ring on reciprocating tests

The performance of usual barrel shaped and flat textured rings were investigated in terms of the cycle averaged friction coefficients. For simplicity, only results concerning the texturing variant 100_10_150, which yielded the highest hydrodynamic load carrying capacity in the previous steady-state simulations, are shown in Fig. 6. Additionally, experimental friction results measured from a reciprocating bench test described in [32] for the barrel shaped ring were also depicted. As expected, the averaged friction coefficients for full texturing were higher than
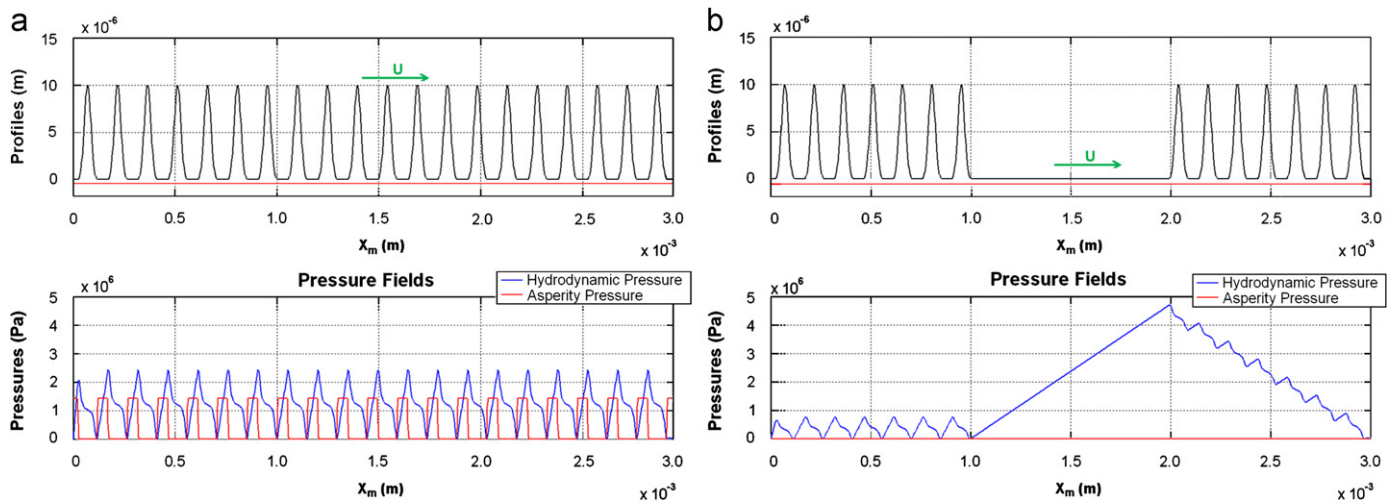
Fig. 4. Texturing geometry (on top) and hydrodynamic and asperity contact pressures for the texturing variant 100_10_150. (a) full texturing (b) partial texturing.
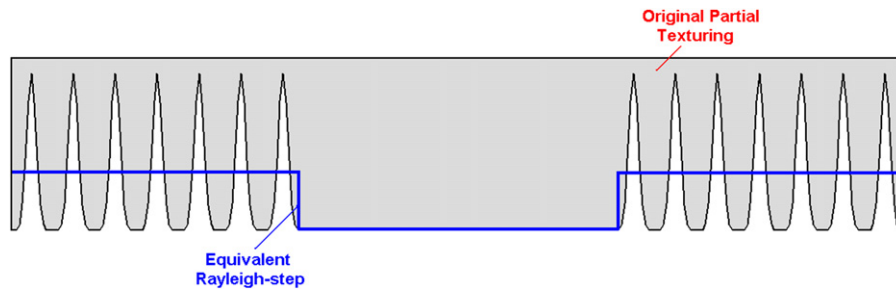

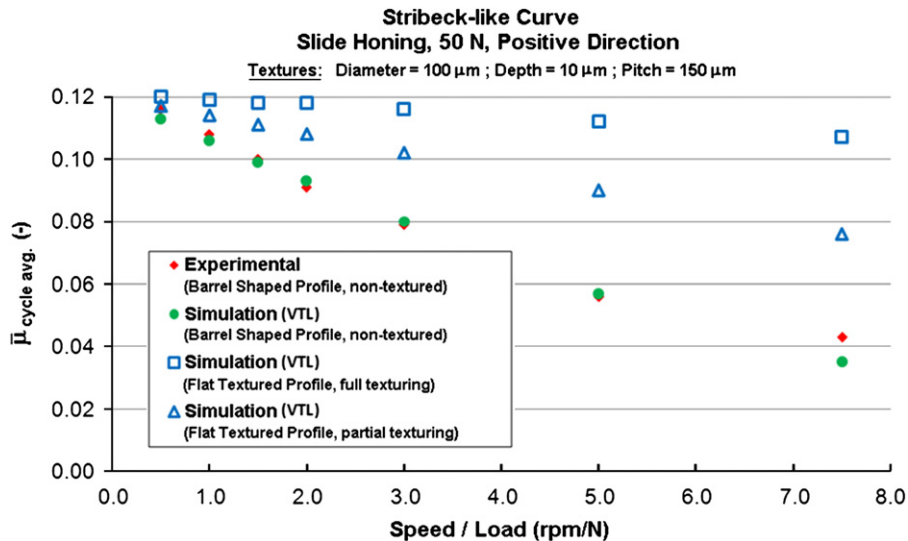**Fig. 5.** "Equivalent Rayleigh-step" created with partial texturing.

Fig. 6. Cycle averaged friction coefficients calculated for the barrel shaped and flat textured profiles.

the partial texturing configuration. However, the calculated friction for the barrel shaped profile was lower than the LST flat variants.

3.3. Comparison between barrel shaped and flat textured piston ring on engine like conditions

Actual operating conditions of a Gasoline Turbo-Charged Engine at 2000 rpm-Full Load (see Table 3) were considered in order to investigate the tribological benefits in terms of the

hydrodynamic support generated by LST on Top and Oil Control Rings. Ring tilt and roughness were neglected; hence only one downward and upward stroke needs to be simulated. Two ring positions along the piston stroke in a combustion engine cycle were analyzed: close to the Top Dead Center (TDC) and at middle stroke.

LST was considered on the rings as well as on the bore. Some combustion engine LST bores are already in production [32]. Applying LST on rings brings the advantage of a smaller region to be textured. On the other hands, due to the ring wear, it can be

expect to last only the break-in. Top and oil control ring wear is about 10–50 μm along the engine life [34]. As the radial wear on the bore is smaller, LST on the bore can be expected to last the engine life. Anyway, the LST effects will be probably reduced as wear progresses, once the depth of the dimples is reduced, either by surface wear or by accumulation of debris or burned oil.

Bore and ring LST were studied separately, i.e. when the bore was textured, the rings were not and vice-versa. For the bore texturing cases, the top ring (3 mm width) was assumed with the typical barrel face profile. As mentioned, the 2-Piece OCR (0.2 mm land width) has a flat face. In partial texturing condition, the non-textured region was placed at the middle of the ring face (similar to Fig. 3). For the OCR land simulations, the dimpled portion was also considered in the middle, which on actual parts would reduce the risk of dimples causing flakes in the land corners. Simulated hydrodynamic support was almost identical for texturing in the face middle or in the borders. Fig. 7 shows the partial LST on the borders and in the middle of the face for the 10_1_15 variant.

The configuration of full stroke LST on the bore was not simulated since it would demand a very large computational mesh, i.e. high computational efforts, for a reasonable discretization of the solution domain. For the bore LST cases, steady-state conditions (hydrodynamic squeeze effect neglected) were simulated according to the data summarized in Table 3. The top and OCR ring faces are small enough to allow a refined computational mesh and a full simulation was carried out. Tables 4 and 5 summarize the simulation results for both texturing combinations described above in terms of the percentage of hydrodynamic support.

Table 3
Engine conditions.

General Parameters	
Speed	2000 rpm
Lubricant	SAE20W50 at 100 °C
Boundary friction	0.12
Bore roughness	As described in Table 1

Conditions close to the TDC		
	Top ring (3 mm width)	OCR (0.2 mm land)
Crank angle	381°	
Position from TDC	3 mm	
Instantaneous velocity	3.53 m/s	
Load pressure (MPA)	6.2	1
Inlet pressure (MPA)	4.2	0
Outlet pressure (MPA)	0.7	0

Conditions on the mid-stroke		
Crank angle	81°	
Position from TDC	37 mm	
Instantaneous velocity	8.14 m/s	
Load pressure (MPA)	0.30	1
Inlet pressure (MPA)	0.15	0
Outlet pressure (MPA)	0.11	0
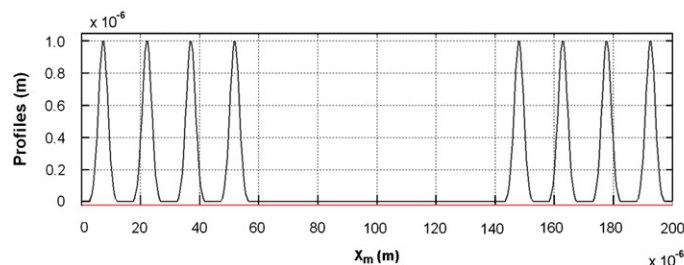
The modelling results showed that the usual face barrel profile on the top ring creates a significant hydrodynamic support. The model predicted 95 and 100% hydrodynamic support, respectively near TDC and at middle stroke. The flat textured variants were unable to produce similar support near TDC and would not be beneficial in terms of friction. These results conflict with some literature using textured surfaces for reducing friction and some remarks should be made:

● For the reciprocating tests, the linear velocities are lower than the ones found in combustion engines and reported in the literature.
● The mathematical model proposed in this work does not take into account the bi-dimensional effects of the lubricant flow against the dimples.

Unlike the top ring, the 2-piece Oil control ring has thin and flat running faces. Some hydrodynamic pressure may arise from the bore topography, as investigated in [35], but hydrodynamic support is low and friction is high. In the current model, such flat face running parallel to the bore is unable to produce any hydrodynamic support. By applying dimples, either on the land face or in the bore, significant hydrodynamic support was
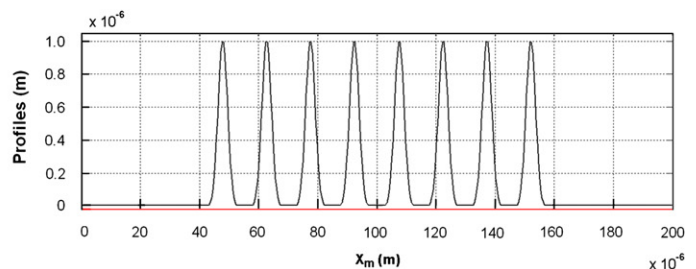
Table 4
Texture on the bore-calculated hydrodynamic support (%).

Dimple dimensions (μm) diameter_depth_pitch	Full or partial LST	3 mm from TDC		Mid-stroke	
		Top ring	2P OCR	Top ring	2P OCR
100_10_150	F	74	50	100	100
	P	89	56	100	98
10_1_15	F	88	16	100	29
	P	91	46	100	79

Table 5
Texture on the rings-calculated hydrodynamic support (%).

Dimple dimension (μm) diameter_depth_pitch	Full or partial LST	3 mm from TDC		Mid-stroke	
		Top ring	2P OCR	Top ring	2P OCR
reference (non-textured)	–	95	0	100	0
100_10_150	F	34	[a]	100	[a]
	P	47	[a]	100	[a]
25_5_50	F	[a]	[a]	[a]	[a]
	P	[a]	29	[a]	64
10_1_15	F	[a]	16	[a]	34
	P	[a]	46	[a]	89

[a] =Not simulated.

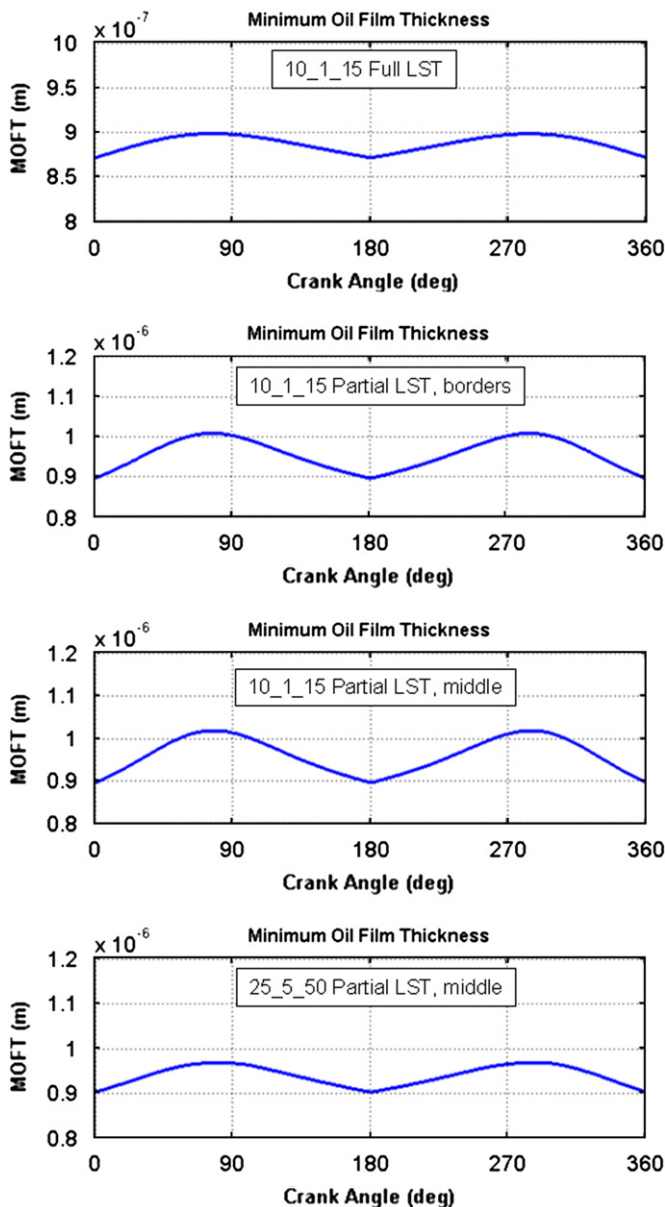**Fig. 7.** LST on the borders and in the middle of the OCR face for the texturing variant 10_1_15.

Fig. 8. Minimum oil film thickness for all LST variants on the OCR.

Fig. 9. Pressure fields along the stroke for the full LST on OCR.
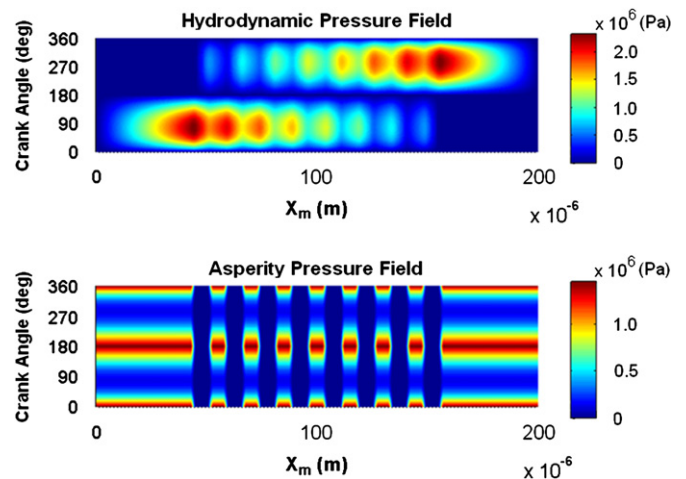
Fig. 10. Pressure fields along the stroke for the partial LST on OCR.

predicted. Such hydrodynamic support in the flat thin lands of the oil ring may reduce wear and friction.

Fig. 8 shows the predicted minimum oil film thickness (MOFT) for the OCR variants. Notice the higher oil film at both reversal point and middle-stroke for the partial variants caused by the generated hydrodynamic pressures on the micro-dimples. For the studied condition, almost no difference was found of using partial texturing at the borders or at the face middle. Among the partial variants, the 10_1_15 showed slight higher films than the 25_5_50. Figs. 9 and 10 show the calculated hydrodynamic and asperity pressures, respectively for the full and the partial LST, along the stroke. Higher hydrodynamic and consequently lower asperity pressures were predicted for the partial texturing. Comparing the hydrodynamic pressure fields, it is evident that "building up" action on the partial LST, while the full LST created only "islands" of hydrodynamic pressure.

Despite the higher hydrodynamic support on the LST variants, calculation of friction by the model brought some surprising results. The calculated friction coefficients were slightly higher than for the non-textured profile. This was caused because in the
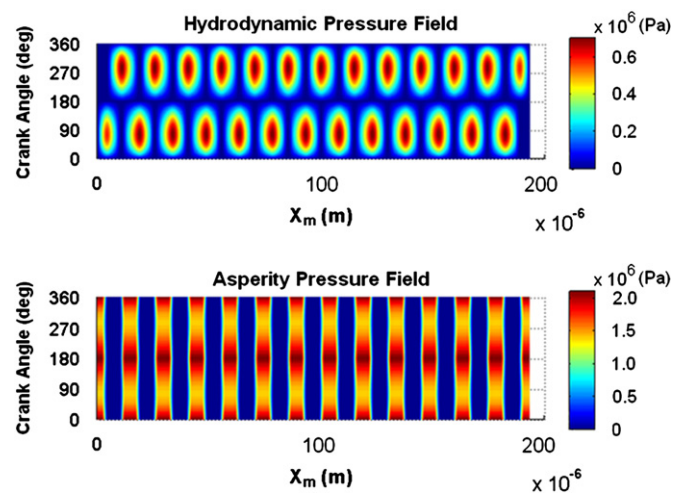
model, when no hydrodynamic pressures is created, all load is supported by the asperity contact and the friction coefficient is limited by the assumed boundary friction coefficient, in this case 0.12. On the other hands, if hydrodynamic pressures are generated, the friction coefficient is calculated according to Eq. (6). For the textured oil control ring, the very thin oil film acting on the flat land portion yielded a friction coefficient higher than the assumed boundary one. An improved hydrodynamic friction model and/or more appropriated assumptions for the boundary friction coefficient are needed and are planned to be addressed together with experiments.

4. Conclusions

A fairly simple computer model was used in order to predict hydrodynamic pressures generated by dimples on bore, top and oil control rings, which allowed the investigation of several texturing variants.

On the bore, LST was able to generate significant hydrodynamic support on the flat, thin, 2P OCR lands, with potential to reduce both friction and wear. For the barrel profile, top ring, effect of bore LST was almost negligible.

LST can also be applied on the oil control ring face. More conventional dimple geometries (100 μm diameter, 10 μm depth) are too large for the OCR land, but smaller dimple dimension,

especially with partial texturing, can be applied. Partial LST produced almost 50% and 90% hydrodynamic support, respectively, near TDC and at middle stroke.

The one-dimensional model was unable to fully predict the complex hydrodynamic phenomena but its low computational effort is beneficial to select the more promising texturing geometries and it provides a simple means to study and understand the main hydrodynamic effects.

References

[1] Grabon W, Pawlus P, Sep J. Tribological characteristics of one-process and two-process cylinder liner honed surfaces under reciprocating sliding conditions. Tribology International 2010;43(10):1882–92.

[2] Etsion I, Kligerman Y, Halperin G. Analytical and experimental investigation of laser-textured mechanical seal faces. Tribology Transactions 1999;42(3):511–6.

[3] Ronen A, Etsion I, Kligerman Y. Friction-reducing surface texturing in reciprocating automotive components. Tribology Transactions 2001;44(3):359–66.

[4] Ryk G, Kligerman Y, Etsion I. Experimental investigation of laser surface texturing for reciprocating automotive components. Tribology Transactions 2002;45(4):444–9.

[5] Brizmer V, Kligerman Y, Etsion IA. Laser surface textured parallel thrust bearing. Tribology Transactions 2003;46(3):397–403.

[6] Ryk G, Kligerman Y, Etsion I, Shinkarenko A. Experimental investigation of partial laser surface texturing for piston rings friction reduction. Tribology Transactions 2005;48(4):583–8.

[7] Kligerman Y, Etsion I, Shinkarenko A. Improving tribological performance of piston rings by partial surface texturing. Tribology Transactions 2005;127(3):632–8.

[8] Ryk G, Etsion I. Testing piston rings with partial laser surface texturing for friction reduction. Wear 2006;261(7-8):792–6.

[9] Etsion I, Halperin G, Becker E. The Effect of Various Surface Treatments on Piston Pin Scuffing Resistance. Wear 2006;261(7-8):785–91.

[10] Etsion I, Sher E. Improving fuel efficiency with laser surface textured piston rings. Tribology International 2009;42(4):542–7.

[11] Wang X, Liu W, Zhou F, Zhu D. Preliminary investigation of the effect of dimples size on friction in line contacts. Tribology International 2009;42(7):1118–23.

[12] Galda L, Pawlus P. Sep J. Dimples shape and distribution effect on characteristics of Stribeck curve. Tribology International 2009;42(10):1505–12.

[13] Tala-Ighil N, Maspeyrot P, Fillon M, Bounif A. Effects of surface texture on journal-bearing characteristics under steady-state operating conditions. proceedings of the institution of mechanical engineers. Part J: Journal of Engineering Tribology 2007;221(6):623–33.

[14] Gao L, Yang P, Dymond I, Fisher J, Jin Z. Effect of Surface texturing on the elastohydrodynamic lubrication analysis of metal-on-metal hip implants. Tribology International 2010;43(10):1851–60.

[15] Takata R, Li Y, Wong V Effects of liner surface texturing on ring/liner friction in large-bore ic engines. ASME-ICEF 2006 Fall Technical Conference, ASME Paper ICEF2006-1525.

[16] Mourier L, Mazuyer D, Lubrecht AA, Donnet C, Audouard E. Action of a femtosecond laser generated micro-cavity passing through a circular EHL contact. Wear 2008;264(5-6):450–6.

[17] Profito FJ, Modelagem Unidimensional do Regime Misto de Lubrificação Aplicada a Superfícies Texturizadas ("One-Dimensional Mixed Lubrication Model Applied to Textured Surfaces"). M.Sc. Dissertation, Polytechnic School, University of São Paulo; 2010.

[18] Profito FJ, Zachariadis D, Tomanik E One Dimensional Mixed Lubrication Regime Model For Textured Piston Rings. Proceedings of 21st Brazilian Congress of Mechanical Engineering 2011 (COBEM 2011).

[19] Frene J, Nicolas D, Degueurce B, Berthe D, Godet M. Hydrodynamic lubrication: bearings and thrust bearings. Amsterdam: Elsevier Science; 1997.

[20] Tian T, Wong VW, Heywood JBA. Piston ring-pack film thickness and friction model for multigrade oils and rough surfaces. SAE Transactions-Journal of Fuels and Lubricants 1996;105:1783–95. (Paper Number 962032).

[21] Akalin O, Newaz GM. Piston ring-cylinder bore friction modeling in mixed lubrication regime: Part I – analytical results. Journal of Tribology 2001;123(1):211–8.

[22] Takata R, Li Y, Wong VW Effects of Lubricant Viscosity on Ring/Liner Friction in Advanced Reciprocating Engine Systems. ASME-ICEF 2006 Fall Technical Conference, ICEF2006-1526.

[23] Peiran Y, Shizhu WA. Generalized Reynolds equation for non-newtonian thermal elastohydrodynamic lubrication. Journal of Tribology 1990;112(4):631–6.

[24] Wang WZ, Liu YC, Wang H, Hu YZA. Computer thermal model of mixed lubrication in point contacts. Journal of Tribology 2004;126(1):162–70.

[25] Wang QJ, Zhu D, Cheng HS, Yu T, Jiang X, Liu S. Mixed lubrication analyses by a macro-micro approach and a full-scale mixed EHL model. Journal of Tribology 2004;126(1):81–91.

[26] Venner CH, Lubrecht AA. Multilevel Methods in Lubrication. Amsterdam: Elsevier Science; 2000.

[27] Qiu Y, Khonsari MM On the Prediction of Cavitation in Dimples Using a Mass-Conservative Algorithm. Journal of Tribology 2009;131(4):041702(11 pages).

[28] Greenwood JA, Tripp JH The Contact of Two Nominally Flat Rough Surfaces. Proceedings of the Institution of Mechanical Engineers 1970;185(1): pp. 625–33.

[29] Tomanik E Modelling of the Asperity Contact Area on Actual 3D Surfaces. SAE Technical Paper Series 2005;SAE2005-01-1864.

[30] Tomanik E, Ferrarese A Use of a Micro-Contact Model to Optimize SI Engine's 3-Piece Oil Rings Profiles Regarding Wear and Lubrication. ASME Technical Paper ICEF2202-526 on ICE-Vol. 39, Design, Application, Performance and Emissions of Modern Internal Combustion Engine Systems and Components.

[31] Tomanik E, Chacon H, Teixeira GA Simple Numerical Procedure to Calculate the Input Data of Greenwood-Williamson Model of Asperity Contact for Actual Engineering Surfaces. Leeds-Lyon Symposium on Tribology: Tribological Research and Design for Engineering Systems, TRIBOLOGY SERIES 2003;41:pp. 205–16.

[32] Tomanik E. Friction and wear bench tests of different engine liner surface finishes. Tribology International 2008;41(11):1032–8.

[33] Tonder K. Inlet roughness tribodevices: dynamic coefficients and leakage. Tribology International 2001;34(12):847–52.

[34] Tomanik E, Nigro F Piston Ring Pack and Cylinder Wear Modelling. SAE Technical 2001; Paper2001-01-0572.

[35] Li Y, Chen H, Tian TA Deterministic Model for Lubricant Transport within Complex Geometry under Sliding Contact and its Application in the Interaction between the OCR and Rough Liner in ICE. SAE Technical Paper Series 2008; SAE2008-01-1615.